Mon. Not. R. Astron. Soc. **000**, 1–15 (2004) Printed 2 February 2008 (MN LATEX style file v2.2)

arXiv:astro-ph/0401392v1 20 Jan 2004

Wide Field Photometry of the Galactic Globular Cluster M 22*†

L. Monaco[1,2]‡, E. Pancino[1], F. R. Ferraro[2], M. Bellazzini[1]

[1] *INAF - Osservatorio Astronomico di Bologna, via Ranzani,1 40127 Bologna, ITALY*
[2] *Dipartimento di Astronomia, Università di Bologna, via Ranzani,1 40127 Bologna, ITALY*

2 February 2008

ABSTRACT

We present wide field photometry of the Galactic Globular Cluster M 22 in the B, V and I passbands for more than 186,000 stars. The study is complemented by the photometry in two narrowband filters centered on H_α and the adjacent continuum, and by infrared J, H and K magnitudes derived from the 2 MASS survey for ∼2000 stars. Profiting from this huge database, we completely characterized the evolved stellar sequences of the cluster by determining a variety of photometric parameters, including new photometric estimates of the mean metallicity, reddening and distance to the cluster. In particular, from our multi-wavelength analysis, we re-examined the long-standing metallicity spread problem in M 22. According to our dataset, we conclude that most of the observed width of the red giant branch must be due to differential reddening, which amounts to a maximum of $\Delta E(B-V) \simeq 0.06$, although the presence of a small metallicity spread cannot be completely ruled out. More specifically, the maximum metallicity spread allowed by our data is of the order of Δ[Fe/H]$\simeq 0.1 \div 0.2$ dex, i.e., not much more than what allowed by the photometric errors. Finally, we identified most of the known variable stars and peculiar objects in our field of view. In particular, we find additional evidence supporting previous optical identifications of the central star of the Planetary Nebula IRAS 18333-2357, which is associated with M 22.

Key words: globular clusters: individual: M 22 – planetary nebulae: individual: IRAS 18333-2357

1 INTRODUCTION

M 22 was one of the first Galactic Globular Clusters (GGC) to be discovered, in 1665, by Abraham Ihle and also one of the first ones to be studied in detail (Shapley 1930; Arp & Melbourne 1959). It soon became the target of a series of studies (starting with Hesser et al. 1977) because of the large color spread of its red giant branch (RGB) sequence, similar to that observed in ω Centauri (Woolley 1966). This suggested the possibility of a metallicity spread in M 22, as was demonstrated in the case of ω Cen a few years before (Dickens & Woolley 1967).

However, while the presence of significant reddening variations was excluded in the case of ω Cen (Cannon 1980), some differential reddening was found in the direction of M 22 (see Richter, Hilker, & Richtler 1999, and references therein). Of course, the presence of differential reddening does not exclude the presence of some metallicity spread, since the two effects could be both present and responsible for the observed width of the RGB. The photometric studies of M 22 by Piotto & Zoccali (1999) and Richter, Hilker, & Richtler (1999) were able to put upper limits to the amount of differential reddening of $\sigma_{\Delta E(V-I)}$=0.05 and ΔE(B−V)=0.07, respectively. Interestingly, Richter, Hilker, & Richtler (1999) demonstrated that part of the spread observed in the Strömgren colours must be due to CH and CN variations, so that the eventual spread in heavy elements should be negligible.

---

* Based on observations made with the European Southern Observatory telescopes, using the Wide Field Imager, as part of the observing program 65.L-0463.
† This publication makes use of data products from the Two Micron All Sky Survey, which is a joint project of the University of Massachusetts and the Infrared Processing and Analysis Center/California Institute of Technology, funded by the National Aeronautics and Space Administration and the National Science Foundation
‡ E-mail: monaco@bo.astro.it

Spectroscopic studies, on the other hand, gave controversial results as far as the heavy elements abundances are concerned, while a spread in the CH and CN abundances of RGB stars appears unquestionable (Norris & Freeman 1983)[1]. For example, some studies reported on metallicity variations of 0.3÷0.5 dex in Ca and/or Fe, often correlated with the CH and CN variations (Peterson 1980; Pilachowski, Leep, Wallerstein, & Peterson 1982; Lehnert, Bell, & Cohen 1991; Brown & Wallerstein 1992), while other studies found no significant variation in the heavy element content (Manduca & Bell 1978; Cohen 1981; Gratton 1982; Gratton & Ortolani 1989; Laird, Wilhelm, & Peterson 1991).

Concerning this apparent contradiction, Lehnert, Bell, & Cohen (1991) noted that, since the the estimated standard deviation of the abundance variations (∼0.2 dex) is close to the typical uncertainty of most spectroscopic analyses, it is very difficult to unequivocally demonstrate the presence of a metallicity spread. This is particularly true if one considers that most of the above studies are only based on a handful of stars ($\leqslant 10$). In the next years, thanks to the new generation of multi-object spectrographs, it will be possible to analyze large samples of stars in a homogeneous way, thus shedding more light on this issue.

M 22 is a metal poor ([Fe/H]≃-1.62, Harris (1996)) and very bright cluster. Considering also its position on the sky, (l; b)=(9.89; -7.55), and its proximity to us (only 3.2 Kpc from the Sun[2]) M 22 is certainly the ideal target for various studies, ranging from the dynamical modelling of dense stellar system (Albrow, De Marchi, & Sahu 2002) to microlensing studies (Sahu et al. 2001). On the other hand the characterization of its stellar content is still quite uncertain since it suffers, once again, from the presence of differential reddening along the line of sight. Here we provide a complete and homogeneous photometric characterization of the stellar content of M 22.

The paper is organized as follows. In Section 2 we present the observations and data reduction procedures, compare our results with previous literature and derive optical and infrared mean ridge lines (MRL). In Section 3 we deal with the differential reddening and metallicity spread issues. In Section 4 we derive the mean metallicity, reddening and distance along with other photometric parameters of M 22. In Section 5 we identify the known variables and peculiar objects, including the central star of the Planetary Nebula IRAS 18333-2357. In Section 6 we summarize our main results.

2 OBSERVATIONS AND DATA REDUCTION

Observations were obtained at the 2.2m ESO/MPI telescope at la Silla, Chile, using the *Wide Field Imager* (WFI), a mosaic of eight 2048×4096 pixels CCDs. The instrument scale is $0\farcs238$ pix^{-1}, giving a total field of view of $34' \times 33'$. A set of B, V and I images were secured during a single observing run on 6-7 July 2000, with exposure times ranging from 5 to 400 sec. We also secured a set of exposures in two narrowband filters, H_α and $\Re$, centered around the H_α line ($\lambda_c \simeq$6580 Å) and on the adjacent continuum ($\lambda_c \simeq$6650 Å). The un-calibrated H_α photometry is briefly discussed in Section 5.1. The average seeing during the observations was $\sim 1''$ full width at half maximum (FWHM).

The raw images were corrected for bias and flat-field using specific IRAF[3] procedures, within the *noao.mscred* package. The photometric reduction was carried out using the DAOPhot II and ALLSTAR packages (Stetson 1987). Stars were searched independently on each CCD of the WFI mosaic with a $3\,\sigma$ threshold and fitted with a second order spatially variable point spread function (PSF).

We used standard IRAF routines to obtain aperture photometry for a sample of isolated stars at various positions along the CCD. We derived the optimal radius for the aperture photometry by constructing the curve of growth of each star. We compared the aperture photometry with the DAOPHOT PSF-fitting photometry and we obtained an aperture correction of 0.00 for the V and I filters (with a typical error of 0.02 and 0.01 respectively) and 0.03 for the B filter (with a typical error of 0.02). The aperture corrections do not correlate with the position of the star on the CCD.

Then we corrected our instrumental magnitudes considering the extinction coefficients available for each filter from the ESO web page[4] and the airmass at the beginning of the observations.

All observations were carried out under photometric conditions. The calibration to the standard Johnson-Cousins photometric system was obtained using two standard fields (namely TPhe and PG 1323, Landolt 1992) observed at different airmasses during the night. The adopted calibrating equations are:

$$\begin{aligned} \mathrm{B} &= b + 0.45\;(b - v) - 0.48 \\ \mathrm{V} &= v - 0.09\;(b - v) - 1.03 \\ \mathrm{I} &= i + 0.12\;(v - i) - 1.88 \end{aligned}$$

where b, v and i are the corrected instrumental magnitudes and B, V and I the corresponding magnitudes in the Johnson-Cousins photometric system.

The resulting, calibrated color magnitude diagrams (CMDs) are displayed on Figures 1 and 2 in the V,(B−V) and V,(V−I) planes, respectively. As can be seen, the population of M 22 dominates the CMD resulting from CCD #2, since the cluster center has been placed on that chip. The bulge and disk populations dominate instead the CMDs of the outer CCDs, where the contribution by M 22 tends to disappear (see, e.g., chips #4 and #5). A few bright stars with V<11.3, (B−V)=1.8 and (V−I)=1.9 are saturated.

Therefore, in the following sections, we will restrict our analysis to stars measured in CCD #2 only, since most of the cluster population lies in that chip, where the contamination by the disk and the bulge is less important and the CMD

---

[1] Some marginal evidence for an over-abundance of *s*-process elements has also been reported by Gratton (1982).

[2] Note that the Galactic Bulge is in the background of M 22.

[3] IRAF is distributed by the National Optical Astronomy Observatories, which is operated by the association of Universities for Research in Astronomy, Inc., under contract with the National Science Foundation.

[4] http://www.eso.org/gen-fac/pubs/astclim/lasilla/index.html, see also: http://www.ls.eso.org/lasilla/sciops/2p2/E2p2M/WFI/zeropoints/

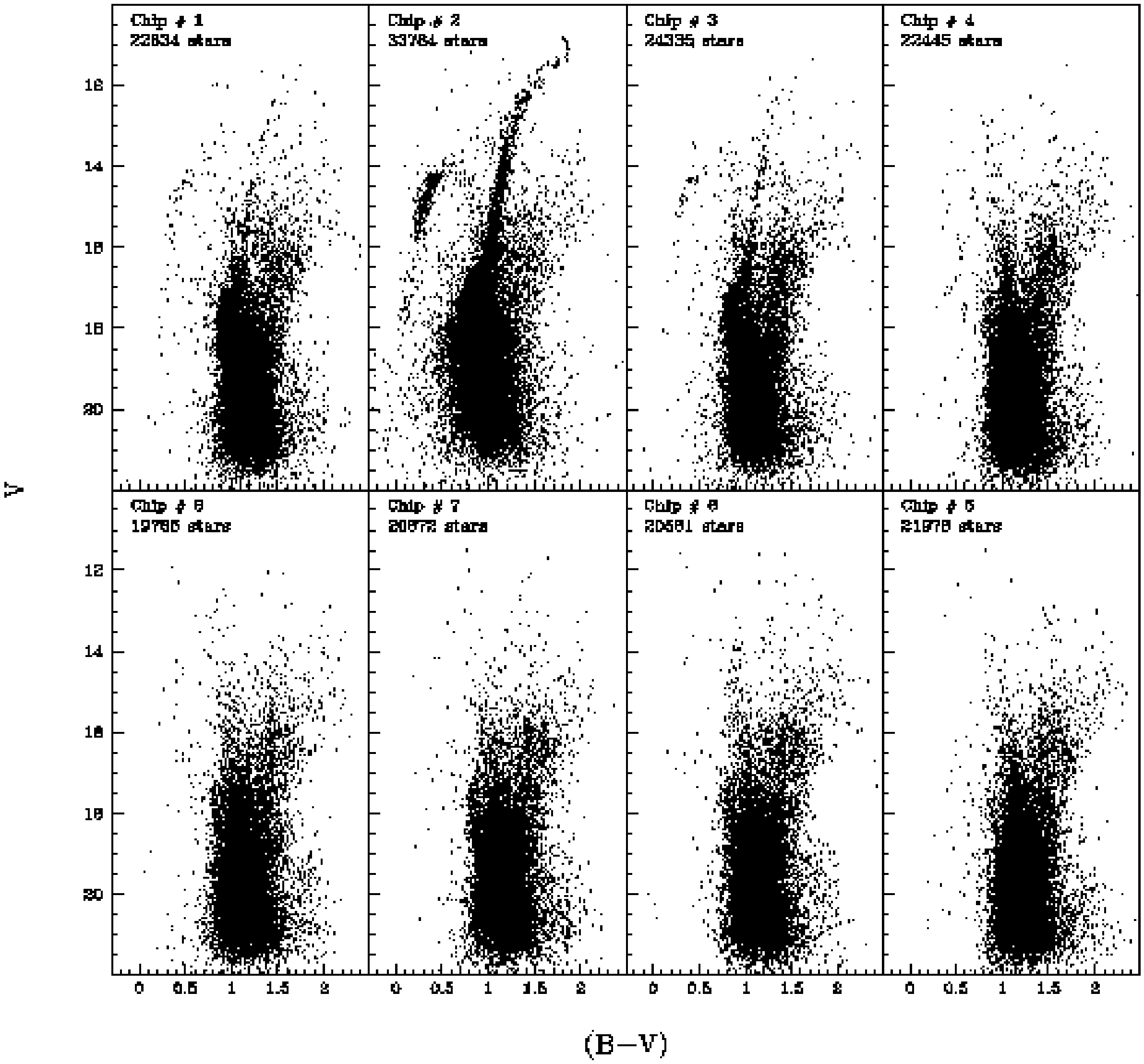

Figure 1. The V *vs* (B-V) CMDs obtained for each of the eight chips of the ESO Wide Field Imager mosaic.

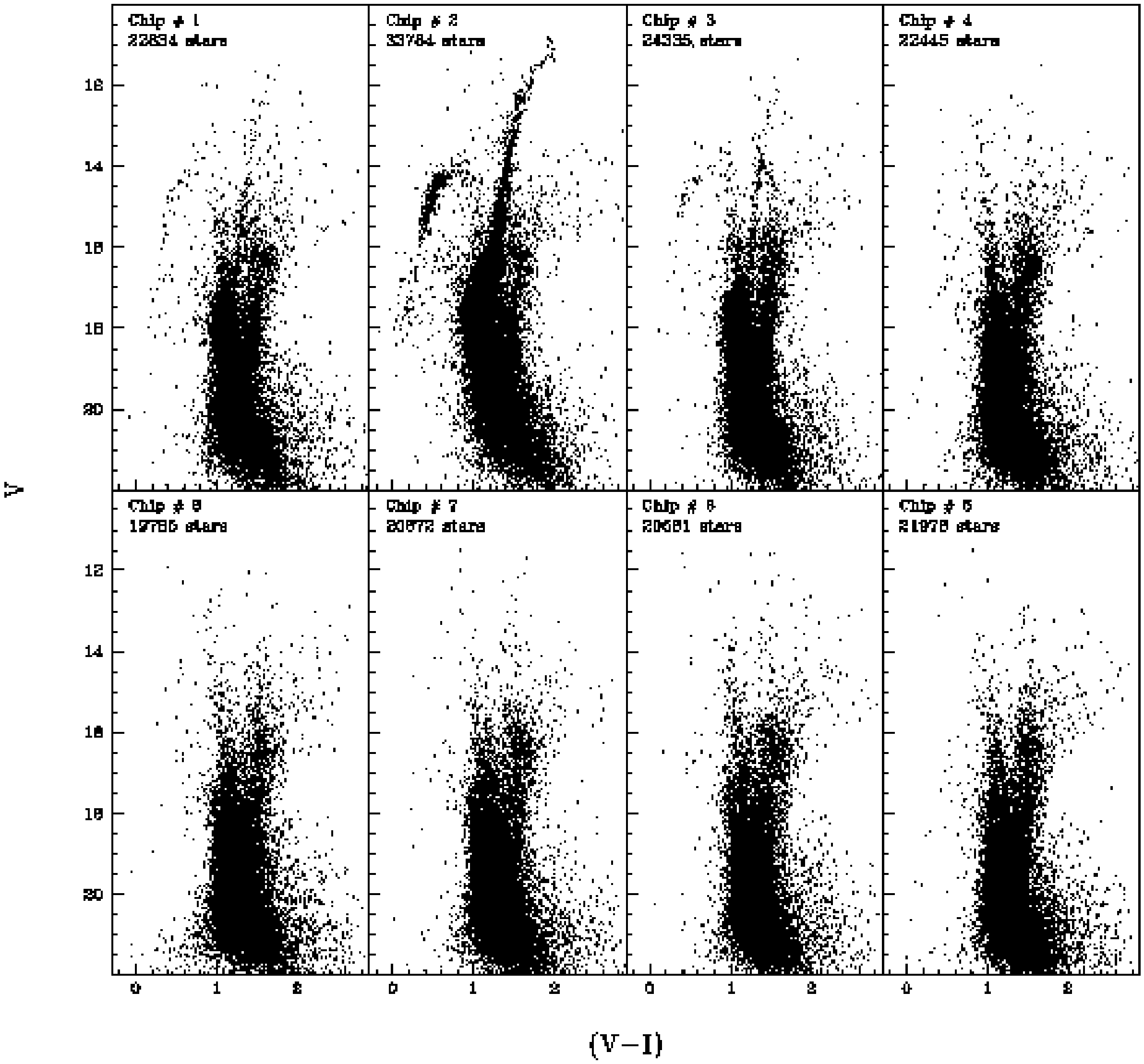

Figure 2. The V *vs* (V-I) CMDs obtained for each of the eight chips of the ESO Wide Field Imager mosaic.

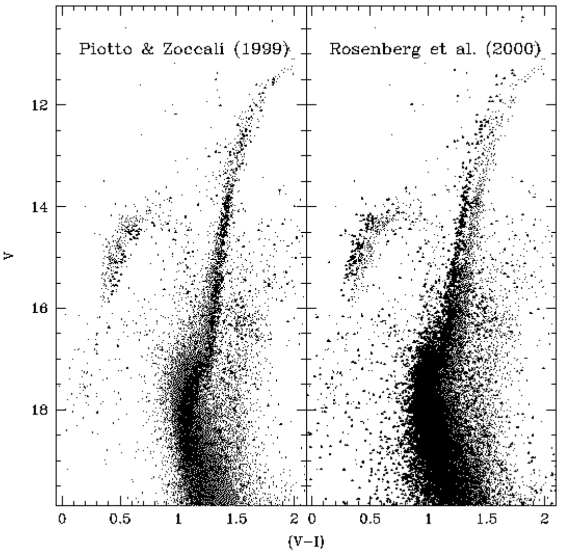

Figure 3. The M 22 photometry by Piotto & Zoccali (1999) (left panel) and by Rosenberg et al. (2000) (right panel) is superposed to the CMD obtained in this paper (light grey).

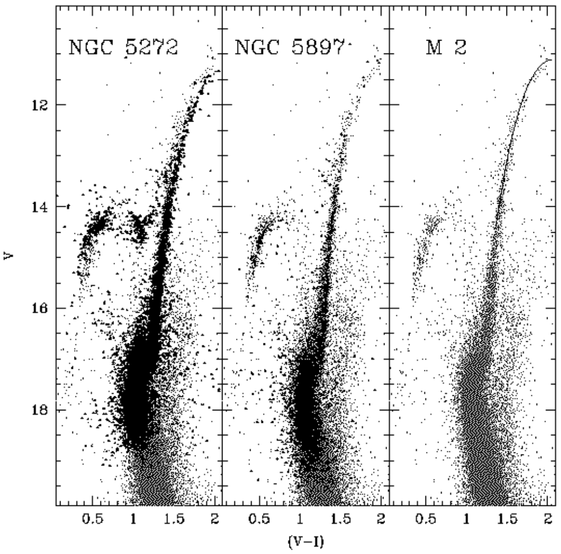

Figure 4. The photometries of NGC 5272 (left panel), NGC 5897 (middle panel) and the mean RGB ridge line of M 2 (right panel) are superposed on our M 22 CMD (light grey). See the text for references.

appears cleaner. This way, we also avoid the propagation of the photometric zero-point differences between different CCDs, which could degrade the overall quality of the photometric catalog.

Finally, in order to complement the multi-wavelenght study of M 22, we identified approximately 1840 stars in our catalogue having J, H and K_s magnitudes measured by the 2 MASS survey[5]. An example of the resulting K_S,(V−K_S) and K_S,(J−K_S) CMDs can be seen in Fig. 7.

2.1 Online Catalogue

Although the following analysis is entirely based on stars belonging to CCD #2, several M 22 stars are still present in CCDs #1, #3, #6, #7 and #8 (Figures 1 and 2). Therefore, the full catalog presented in Table 1 and published electronically contains all the stars detected in these CCDs.

The catalog contains the B, V, I calibrated magnitudes on columns #2, #4, #6, each followed by the formal daophot errors (δB, δV, δI). Only stars measured both in the V and I filters are tabulated while the B magnitude is provided only when available. A flag "0.000" can be found on columns #2 and #3 if a star is not measured in the B filter.

Star positions are provided both in the pixel coordinate system of each CCD (columns #7, #8) and in the equatorial (RA; Dec) coordinate system (columns #9, #10). In the first column we provide a sequential identifier for each star.

The coordinates in the J2000.0 absolute astrometric system have been obtained with a procedure already described in other papers (see e.g. Ferraro et al. 2001). The new astrometric *Guide Star Catalog* (GSC II) recently released and now available on the web[6], was used as reference. More than two thousand GSC II astrometric reference stars have been found in the field of view of each chip, allowing for an accurate absolute positioning of the image. In order to derive an astrometric solution for each WFI CCD, we used a program specifically developed at the Bologna Observatory (P. Montegriffo et al 2004, in preparation). As a result of the entire procedure, r.m.s. residuals of $\sim 0\farcs2$, both in RA and Dec, were obtained. This value can be considered as a representative uncertainty of the astrometric calibration procedure.

The photometry of stars belonging to CCDs #1, #3, #6, #7 and #8 has been shifted to match the photometry of CCD #2, taking into account the different CCD responses. The correction was calculated by fitting the mean ridge lines calculated in §2.3 to the CMDs. The correction applied to each of the B, V, I magnitudes of the external chips is always $\leqslant$0.1 mag. However, in the CMD of chips #6, #7 and #8, only a handful of cluster stars is present in the main

---

[5] http://www.ipac.caltech.edu/2mass

[6] http://www-gsss.stsci.edu/gsc/gsc2/GSC2home.htm

Table 1. CCD B, V, I online photometric catalog of M 22. Only a few entries are displayed to illustrate the catalog format and contents.

Chip#2										
Star Id	B	δB	V	δV	I	δI	X_{pix}	Y_{pix}	RA	Dec
1	12.071	0.010	10.351	0.010	8.544	0.124	806.273	1876.142	279.11637069	−23.92032070
2	10.854	0.010	10.483	0.011	9.938	0.014	1808.769	4086.802	279.04357491	−23.77422799
3	12.632	0.010	10.835	0.010	8.925	0.015	1221.985	1819.724	279.08629030	−23.92412172
4	12.707	0.010	10.885	0.010	8.936	0.018	1806.331	1933.347	279.04400418	−23.91672994
5	12.793	0.010	10.941	0.010	8.979	0.015	52.285	1092.889	279.17106212	−23.97201436
6	12.888	0.010	11.043	0.010	9.123	0.015	1406.258	2075.037	279.07292590	−23.90726310
7	12.958	0.010	11.095	0.010	9.096	0.018	333.186	757.506	279.15076070	−23.99417931

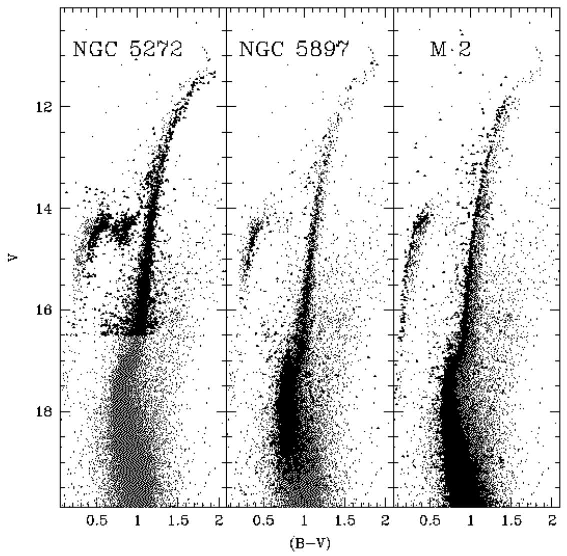

Figure 5. The photometries of NGC 5272 (left panel), NGC 5897 (middle panel) and M 2 (right panel) are superposed on our M 22 CMD (light grey). See the text for references.

sequence and turn off regions and the calculated corrections are correspondingly less certain.

2.2 Literature Comparisons

In order to check our calibration, we compared our V,(V−I) photometry with two catalogues previously published by Piotto & Zoccali (1999) and Rosenberg et al. (2000).

Fig. 3 shows the results of such a comparison. In particular, the photometry by Piotto & Zoccali (1999) appears in good agreement with ours as far as the upper RGB is concerned (left panel of Fig. 3). However, their horizontal branch (HB) appears *redder* and *fainter* than ours, by approximately 0.18 dex in magnitude and 0.04 dex in color. A similar discrepancy can be observed for the lower RGB and the turn-off (TO) regions, pointing towards a possible residual (V−I) color-term between the two calibrations. On the other hand, the comparison with Rosenberg et al. (2000) results again in a discrepancy, but in the opposite sense (right panel of Fig. 3). Both the RGB and HB appear in fact systematically *bluer* and *brighter* than ours, by roughly 0.1 dex in color and 0.05 dex in magnitude. In this case, there appears to be a residual zero-point difference between the two calibrations.

To further investigate on this issue, we compared (Fig. 4) our photometry with that of three globular clusters having similar metallicities (and thus similar RGB shapes) as M 22. More specifically, the left panel of Fig. 4 shows the comparison of our M 22 photometry with that of NGC 5272 (Ferraro et al. 1992), which has a metallicity of $[Fe/H]_{ZW}$=-1.66 in the Zinn & West (1984) scale. NGC 5272 has been corrected with the reddening and distance tabulated by Ferraro et al. (1999) and with the corresponding values for M 22 (see Section 4). The middle panel of Fig. 4 shows the comparison with NGC 5897 (Ferraro et al. 1997), which has $[Fe/H]_{ZW}$=-1.68 and has been corrected for reddening and distance as above. Finally, the right panel of Fig. 4 shows the comparison of our M 22 photometry with the RGB mean ridge line of M 2, which has $[Fe/H]_{ZW} = -1.62$ (Harris 1996) and was published by Da Costa & Armandroff (1990) already corrected for reddening and distance. We thus applied the distance modulus and reddening of M 22 following Harris (1996), to be consistent with the distance scale of Da Costa & Armandroff (1990).

As can be seen, all the three panels of Fig. 4 show an excellent match with the present photometry of M 22, thus dispelling any remaining doubt on the adopted absolute V and I calibration.

Unfortunately, among the recent CCD studies of M 22, the only available B-band dataset is the one by Kaluzny & Thompson (2001) and, as the authors explicitely state in their paper, their *absolute* photometric calibration is not reliable. In Fig. 5 we compared our photometry to that of NGC 5272, NGC 5897 (Ferraro et al. 1999) and M 2 (Lee & Carney 1999) in the V *vs* B-V plane. The CMDs of NGC 5272 and NGC 5897 have been corrected exactly as in Fig. 4. The M 2 CMD have been corrected for the appropriate reddening and distance and the corresponding M 22 values tabulated by Harris (1996). We find a reasonable agreement with each of the reference clusters and we conclude that also our B-band calibration can be considered reliable. In particular, a good match is obtained in the case of NGC 5897 and of the RGB of NGC 5272. The NGC 5272

HB is redder than the M 22 one even if the mean level appears similar. We also obtain a reasonable agreement in the case of M 2, even if its CMD is somewhat bluer than the M 22 one.

2.3 Optical and IR Mean Ridge Lines

Profiting from this large photometric database, we have constructed the RGB mean ridge lines for M 22, both in the optical and infrared colors. Since the optical photometry is deeper than the infrared 2 MASS photometry, we were able to reach down to the main sequence in the V,(V−I) and V,(B−V) planes, while we reach the base of the RGB in the K,(V−K_S) and K,(J−K_S) planes (see Fig. 7).

To derive the lines, we sliced the sequences in appropriate magnitude and/or color bins of variable size (depending on the number of points and on the shape of the sequence). The representative point of each bin has been computed as the $2\,\sigma$ clipped average. The set of representative points has then been fitted by analytical polynomials of variable degree until the best-fitting polynomial was found. The resulting mean ridge lines are tabulated in Tables 2 (optical) and 3 (optical-infrared) and they are overplotted on the respective CMDs, in Fig. 7.

The morphology of the M 22 RGB in the infrared passbands was studied by Davidge & Harris (1996). These authors noted a pronounced discrepancy in the lower RGB between their M 22 (K, J-K) fiducial line and that of M 13 (Davidge & Harris 1995), a cluster of similar metallicity (Harris 1996). We compared the shape of our (K_S, J-K_S) fiducial line (converted to the standard system using the relation of Carpenter 2001) to the one of M 13 published by Davidge & Harris (1995) and we find a reasonable agreement among the two ridge lines (see figure 6).

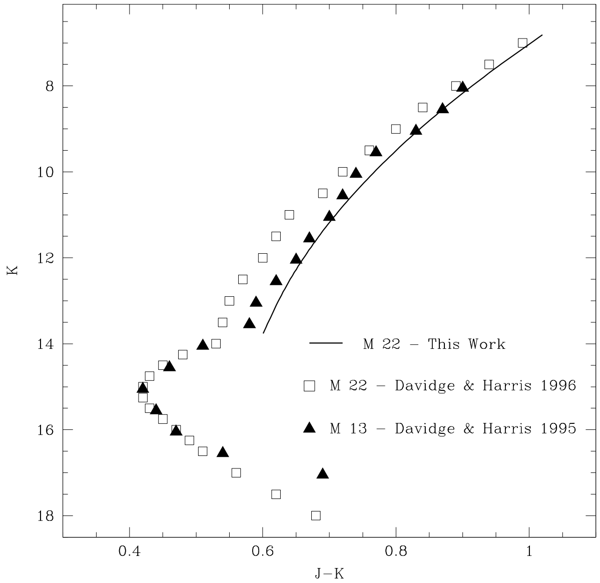

Figure 6. Our M 22 infrared mean ridge line (continuous line) is compared with the M 22 and M 13 normal points by Davidge & Harris (1996) (open squares) and Davidge & Harris (1995) (filled triangles), respectively. We applied horizontal and vertical shifts to align M 13 to the M 22 normal points at the turn off and the point 0.05 mag redward of the turn off, just as done by Davidge & Harris (1996) (see lower panel in their figure 7).

3 DIFFERENTIAL REDDENING AND METALLICITY SPREAD

The most striking characteristic of the CMD of M 22 is the large color spread of the RGB, incompatible with measurement errors. As summarized in Section 1, there is a long-standing debate about a possible metallicity spread in M 22, but the well established presence of some differential reddening (Richter, Hilker, & Richtler 1999) in the direction of M 22 further complicates the analysis, since both mechanisms can contribute to widen the RGB in color and they are difficult to disentangle.

The presence of differential reddening is easily demonstrated in Fig. 8. As can be seen, stars on the red and blue sides of the mean ridge lines derived in Section 2.3 occupy different spatial positions in the cluster. In particular, stars *redder* than the mean ridge line tend to populate preferentially the uppermost part of CCD #2 (i.e., North of the cluster center). The opposite is true for stars *bluer* than the mean ridge line. Thus, the northern part of the cluster must be more reddened than the southern part. The same kind of behaviour can be observed using the HB sequence, which is less sensitive to metallicity than the RGB, confirming that the dominant contribution to the color spread of both sequences must be due to reddening variations. However, we still cannot exclude the presence of some (small) degree of metallicity spread. From a careful inspection of Figure 8, it is also evident that differential reddening is present on different scales, ranging from ∼100 pix (see the *"hole"* at (X, Y) = (600, 1100) in the lower-left panel) to ∼1000 pix (see the lower half of the lower-left panel). Therefore, a wide field study is also required in order to obtain mean properties that are really representative of M 22.

Here, we profited from our multi-band photometry to put quantitative constraints to the amount of metallicity spread allowed by the color spread of the RGB. In particular, we studied the RGB color distribution of M 22 in (B−V), (V−I) and (V−K_S), selecting stars with V$\leqslant$15 for (B−V) and (V−I), and stars with $K_S\leqslant$12 for (V−K_S). This is necessary to avoid any contamination from the galactic bulge and to use only measurements with the highest possible signal-to-noise ratio. We then computed the color difference, at fixed magnitude, between each star and the corresponding mean ridge line (Section 2.3). The histograms of the resulting differences are plotted in Fig. 9 for each color. A gaussian curve representing the measurement errors is overplotted on each histogram (dot-dashed curve). A gaussian fit to the actual color dispersion is also overplotted (solid curve) on each histogram. The latter gaussian shows of course a larger dispersion than the one representing the errors only, since it contains also the contribution of the intrinsic spread, i.e. the differential reddening plus the eventual metallicity dispersion[7].

---

[7] We point out the presence of a clump of stars with redder colors in Fig. 9, especially visible in (B−V). If the colors of these stars

Table 2. Optical M 22 mean ridge lines

V	(B–V)	(V–I)	V	(B–V)	(V–I)	V	(B–V)	(V–I)	V	(B–V)	(V–I)	V	(B–V)	(V–I)
11.25	1.752	1.928	13.49	1.203	1.452	15.68	1.040	1.298	17.47	0.812	1.060	18.57	0.845	1.117
11.38	1.703	1.877	13.60	1.190	1.444	15.78	1.034	1.293	17.52	0.809	1.059	18.62	0.851	1.122
11.49	1.659	1.830	13.69	1.181	1.436	15.87	1.029	1.287	17.57	0.805	1.058	18.67	0.857	1.127
11.60	1.621	1.796	13.78	1.171	1.429	15.97	1.024	1.283	17.62	0.803	1.057	18.72	0.862	1.133
11.69	1.593	1.763	13.89	1.159	1.422	16.07	1.019	1.278	17.67	0.801	1.057	18.78	0.870	1.140
11.79	1.561	1.733	13.99	1.149	1.415	16.18	1.013	1.273	17.73	0.800	1.057	18.82	0.874	1.144
11.89	1.528	1.705	14.08	1.141	1.409	16.27	1.008	1.269	17.77	0.799	1.058	18.86	0.880	1.149
11.99	1.496	1.679	14.18	1.135	1.402	16.37	1.002	1.264	17.82	0.800	1.059	18.92	0.888	1.156
12.09	1.470	1.654	14.27	1.128	1.395	16.47	0.997	1.259	17.87	0.800	1.061	18.99	0.897	1.164
12.18	1.446	1.632	14.38	1.118	1.388	16.57	0.993	1.255	17.92	0.802	1.063	19.03	0.903	1.169
12.27	1.423	1.610	14.48	1.111	1.380	16.68	0.988	1.246	17.97	0.803	1.065	19.07	0.909	1.175
12.38	1.397	1.591	14.57	1.105	1.373	16.77	0.982	1.236	18.02	0.805	1.068	19.11	0.915	1.180
12.47	1.374	1.573	14.67	1.098	1.364	16.88	0.969	1.224	18.07	0.809	1.072	19.21	0.929	1.194
12.57	1.354	1.557	14.78	1.093	1.356	16.97	0.950	1.211	18.12	0.811	1.076	19.31	0.944	1.209
12.67	1.333	1.541	14.87	1.087	1.350	17.08	0.912	1.171	18.17	0.814	1.080	19.41	0.959	1.225
12.76	1.315	1.527	14.97	1.080	1.342	17.14	0.885	1.111	18.22	0.817	1.085	19.50	0.971	1.237
12.86	1.297	1.515	15.08	1.074	1.335	17.17	0.875	1.098	18.27	0.820	1.090	19.60	0.985	1.255
12.95	1.281	1.503	15.17	1.069	1.329	17.22	0.860	1.082	18.32	0.823	1.094	19.70	0.998	1.273
13.06	1.263	1.492	15.27	1.063	1.323	17.27	0.845	1.075	18.37	0.827	1.098	19.80	1.011	1.291
13.16	1.249	1.482	15.38	1.056	1.316	17.32	0.833	1.070	18.42	0.831	1.103	19.91	1.023	1.310
13.28	1.230	1.470	15.49	1.050	1.311	17.37	0.824	1.065	18.47	0.835	1.108	20.01	1.031	1.330
13.40	1.214	1.460	15.58	1.045	1.305	17.42	0.817	1.062	18.52	0.839	1.112			

Table 3. Infrared and Optical-Infrared M 22 mean ridge lines

K_S	$(V–K_S)$	$(J–K_S)$	K_S	$(V–K_S)$	$(J–K_S)$	K_S	$(V–K_S)$	$(J–K_S)$	K_S	$(V–K_S)$	$(J–K_S)$	K_S	$(V–K_S)$	$(J–K_S)$
6.814	4.269	1.020	8.234	3.723	0.895	9.653	3.319	0.790	11.07	3.075	0.706	12.49	2.863	0.641
6.888	4.240	1.013	8.308	3.698	0.889	9.728	3.303	0.785	11.15	3.064	0.702	12.57	2.850	0.639
6.963	4.210	1.006	8.383	3.672	0.883	9.803	3.287	0.780	11.22	3.054	0.698	12.64	2.837	0.636
7.038	4.180	0.999	8.458	3.647	0.877	9.878	3.272	0.775	11.30	3.043	0.694	12.72	2.824	0.633
7.113	4.150	0.992	8.533	3.623	0.871	9.952	3.257	0.771	11.37	3.033	0.690	12.79	2.811	0.631
7.187	4.120	0.985	8.607	3.599	0.865	10.03	3.243	0.766	11.45	3.023	0.687	12.87	2.797	0.628
7.262	4.090	0.979	8.682	3.576	0.860	10.10	3.229	0.761	11.52	3.012	0.683	12.94	2.784	0.626
7.337	4.061	0.972	8.757	3.553	0.854	10.18	3.215	0.757	11.60	3.002	0.680	13.02	2.771	0.623
7.412	4.031	0.965	8.831	3.531	0.848	10.25	3.202	0.752	11.67	2.991	0.676	13.09	2.757	0.621
7.486	4.002	0.958	8.906	3.509	0.843	10.33	3.189	0.748	11.75	2.980	0.673	13.17	2.744	0.618
7.561	3.973	0.952	8.981	3.487	0.837	10.40	3.176	0.743	11.82	2.969	0.669	13.24	2.731	0.616
7.636	3.944	0.945	9.056	3.467	0.832	10.48	3.164	0.739	11.90	2.958	0.666	13.32	2.718	0.614
7.710	3.915	0.939	9.130	3.446	0.826	10.55	3.152	0.734	11.97	2.947	0.663	13.39	2.706	0.612
7.785	3.887	0.932	9.205	3.427	0.821	10.62	3.141	0.730	12.04	2.936	0.660	13.46	2.694	0.610
7.860	3.858	0.926	9.280	3.407	0.816	10.70	3.129	0.726	12.12	2.924	0.656	13.54	2.682	0.607
7.935	3.831	0.920	9.355	3.389	0.810	10.77	3.118	0.722	12.19	2.912	0.653	13.61	2.671	0.605
8.009	3.803	0.913	9.429	3.370	0.805	10.85	3.107	0.718	12.27	2.900	0.650	13.69	2.662	0.603
8.084	3.776	0.907	9.504	3.353	0.800	10.92	3.096	0.714	12.34	2.888	0.647	13.76	2.653	0.601
8.159	3.750	0.901	9.579	3.336	0.795	11.00	3.085	0.710	12.42	2.876	0.644			

We can then represent the observed color dispersion, $\sigma_{(M_1-M_2)_{obs}}$, as the sum of three terms, one due to photometric errors, $\sigma_{\delta(M_1-M_2)}$[8], the second to the differential reddening, $\sigma_{\Delta E(M_1-M_2)}$, and the third to the intrinsic metallicity spread, $\sigma_{\Delta[\mathrm{M/H}]}$

$$\begin{aligned} \sigma^2_{(M_1-M_2)_{obs}} &= \sigma^2_{\delta(M_1-M_2)} + \sigma^2_{\Delta E(M_1-M_2)} + \sigma^2_{\Delta[M/H]} \\ &= \sigma^2_{\delta(M_1-M_2)} + \sigma^2_{(B-V)_{int}} \end{aligned}$$

Since the observed color spreads and the photometric errors are

$$\begin{aligned} \sigma_{(B-V)_{obs}} &= 0.026; & \sigma_{\delta(B-V)} &= 0.015 \\ \sigma_{(V-I)_{obs}} &= 0.030; & \sigma_{\delta(V-I)} &= 0.016 \\ \sigma_{(V-K_S)_{obs}} &= 0.055; & \sigma_{\delta(V-K_S)} &= 0.030 \end{aligned}$$

---

are due to differential reddening, they could be tracing a denser interstellar matter region, with an E(B−V) which is ∼0.06 mag higher than the average cluster reddening.

[8] Photometric errors are computed as the standard deviation of repeated measurments of a star magnitude, available for the B, V, and I filters. In the case of the K_S filter, we used errors provided by the 2 MASS extraction algorithm. We excluded stars belonging to the inner 1′ around the cluster center, where crowding effects are most severe.

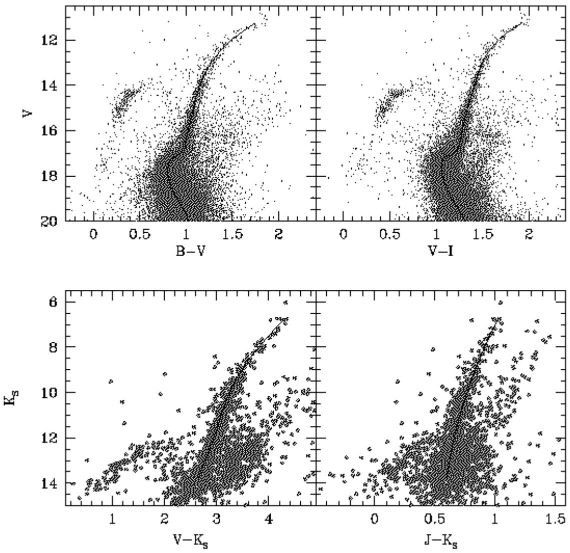

Figure 7. The mean ridge lines listed in Table 2 and 3 are superposed to the CMDs in the optical (upper panels), infrared (lower-right panel) and optical-infrared planes (lower-left panel).

we can derive the intrinsic color spreads obtaining:

$$\sigma_{(B-V)_{int}} = \sqrt{\sigma^2_{\Delta E(B-V)} + \sigma^2_{\Delta[\mathrm{M/H}]}} = 0.02$$

$$\sigma_{(V-I)_{int}} = \sqrt{\sigma^2_{\Delta E(V-I)} + \sigma^2_{\Delta[\mathrm{M/H}]}} = 0.03$$

$$\sigma_{(V-K_S)_{int}} = \sqrt{\sigma^2_{\Delta E(V-K_S)} + \sigma^2_{\Delta[\mathrm{M/H}]}} = 0.05$$

These values have to be considered as *upper limits* to the amount of differential reddening needed to explain the RGB width, if we assume zero metallicity spread. The above values are in reasonable agreement with previous determinations. In fact, $\sigma_{\Delta E(V-I)}$=0.05, derived by Piotto & Zoccali (1999) using the main sequence, compares reasonably with our $\sigma_{\Delta E(V-I)}$=0.03, while ΔE(B−V)=(0.07;0.08), derived respectively by Richter, Hilker, & Richtler (1999) and Anthony-Twarog, Twarog, & Craig (1995) from Strömgren photometry, compares very well with our ΔE(B−V)≃ $3 \cdot \sigma_{\Delta E(B-V)}$=0.06.

We also note that the intrinsic spread, in the three different colors, changes following the reddening laws (in the following we will always use the reddening laws by Dean, Warren & Cousins (1978) and Savage & Mathis (1979)). In fact, assuming $\sigma_{\Delta E(B-V)}$=0.02 as above, we obtain $\sigma_{\Delta E(V-I)}$ and $\sigma_{\Delta E(V-K_S)}$ that are virtually identical to the values derived above

$$\sigma_{\Delta E(V-I)} = 1.34 \cdot \sigma_{\Delta E(B-V)} = 0.03$$

$$\sigma_{\Delta E(V-K_S)} = 2.72 \cdot \sigma_{\Delta E(B-V)} = 0.06$$

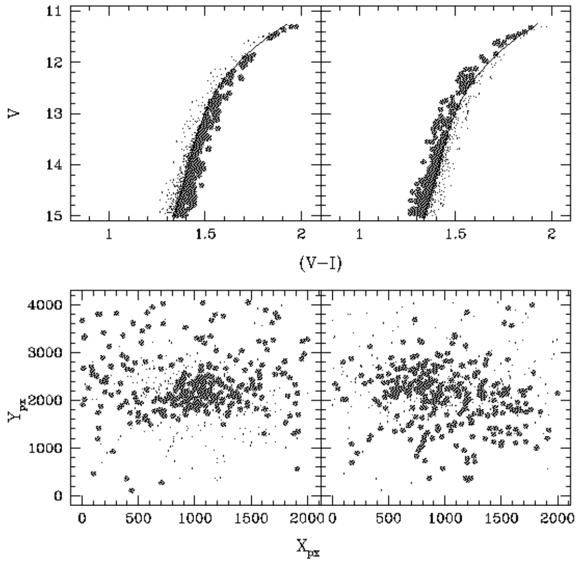

Figure 8. The stars in the M 22 RGB are divided into two samples, according to their position with respect to the mean ridge line (upper panels). The stars in the two sample have different spatial distributions (lower panels).

Therefore, since the intrinsic width of the RGB scales from the optical planes to the optical-infrared plane exactly as expected from the reddening laws, we have to conclude that the room left for an intrinsic metallicity spread must be very small.

To confirm this conclusion, we made use of two reddening free color indices

$$Q_{BVI} = (B-V) - \frac{E(B-V)}{E(V-I)}(V-I)$$

$$Q_{BVK} = (B-V) - \frac{E(B-V)}{E(V-K_S)}(V-K_S)$$

and we plotted them in the top panel of Fig. 10. The position of stars in the (Q_{BVI}, Q_{BVK}) plane should thus depend only on the intrinsic properties of the stars (i.e., temperature and chemical composition). In particular, the spread around the mean locus should depend only on the eventual metallicity spread and on the photometric errors, since the Q-color indices are independent on reddening by definition.

Therefore, we derived the mean ridge line of the locus in Fig. 10 (thick line) with the same method used in Section 2.3. We measured the distance of each star from the mean ridge line and we constructed the histogram shown in the bottom panel of Fig. 10. Two gaussians have been overplotted: the one obtained by propagating the photometric errors to the (Q_{BVI}, Q_{BVK}) plane (dotted-dashed line) and the one that best-fits the distribution (solid line). As can be seen, the two gaussians are virtually identical.

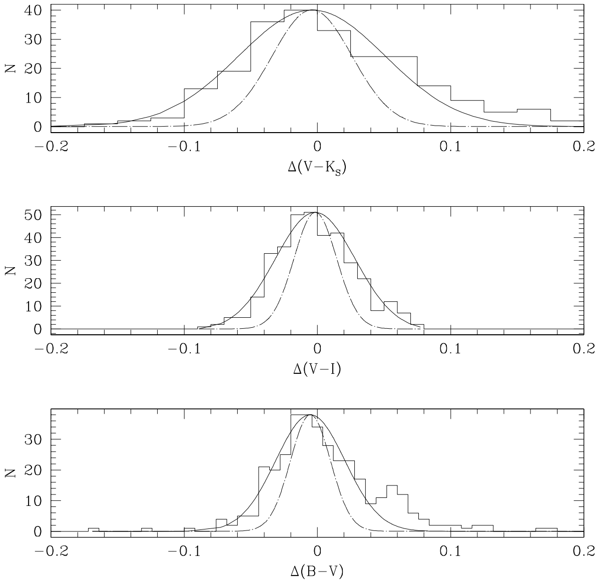

Figure 9. The observed color difference distribution between stars in the RGB and the corresponding mean ridge line is plotted in B-V (lower panel), V-I (middle panel) and V-K$_S$ (upper panel). Two gaussian curves representing the fit to the observed distribution (continuous curve) and the distribution expected by photometric errors (dot-dashed curve) are also plotted on each panel.

Summarizing, the metallicity spread contribution to the intrinsic width of the RGB must be smaller than our typical measurement errors, i.e., of the order of $\sim 0.01 \div 0.02$ mag. Using equation 8 in Carretta & Bragaglia (1998) and considering (V-I)$_{0,g}$=0.92 (see next section), we derive that a color spread of $\sim$ 0.01 ÷ 0.02 corresponds to a metallicity spread of approximately Δ[Fe/H]$\simeq$ 0.1 ÷ 0.2 dex, which is the maximum metallicity spread allowed by the present photometry. This spread is also of the order of the uncertainty of high-resolution abundance determinations for a single star (∼0.15 dex). Therefore such a low metallicity spread, if present, could remain hidden into the instrumental errors even studying a large sample of high resolution spectra of M 22 stars.

4 METALLICITY, REDDENING AND DISTANCE

In this Section we characterize the photometric properties of the stellar population in M 22 by measuring the complete set of observables for the evolved sequences, with the aim of obtaining modern, CCD based estimates of the cluster mean metallicity, mean reddening and distance modulus.

The V$_{ZAHB}$ level was obtained from the comparison of the observed star distribution along the HB with synthetic HB of appropriate metallicity ($[M/H] \sim -1.5$, see below), following the semi-empirical approach described by Ferraro et al. (1999). This method is extremely robust since it allows the direct determination of V$_{ZAHB}$, instead of relying on the mean HB level as an indicator of the ZAHB level. We obtained

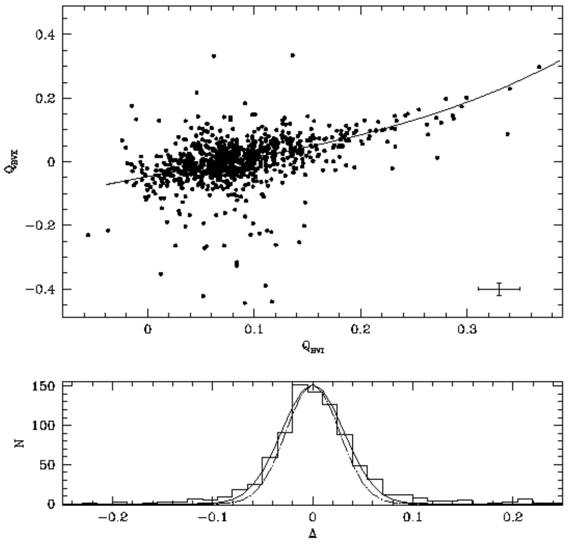

Figure 10. RGB stars in M22 are plotted in the plane of the two reddening free color indices Q$_{BVI}$ *vs* Q$_{BVK}$ (upper panel). The continuos curve is the mean locus of stars in the plane. In the lower panel the observed distribution of the stars distances from the mean locus is plotted (histogram). The two gaussian curves represent a fit to the observed distribution (continuos curve) and the distribution expected considering the photometric errors (dotted-dashed curve).

$$V_{ZAHB} = 14.33 \pm 0.05$$

about 0.15 mag fainter than what reported by Harris (1996). This is easily understood in view of the fact that the Harris (1996) value is referred to the mean HB level instead of the Zero Age Horizontal branch level (see equation #2 in Ferraro et al. 1999).

Rosenberg et al. (2000) derived V$_{ZAHB}$ =14.25 for M 22 and, considering the zero point difference with our V magnitudes (0.05, see section 2.2), our V$_{ZAHB}$ level results to be about 0.03 magnitude fainter than their value.

Next, we proceeded to the simultaneous determination of the mean metallicity and reddening, using a procedure that was first introduced by Sarajedini (1994). In its original description, the method allowed the derivation of [Fe/H] in the Zinn & West (1984) scale, using V,(V−I) photometries and mean ridge lines of the RGB. Later, the procedure was calibrated to the Carretta & Gratton (1997) scale by Carretta & Bragaglia (1998) and extended to the B,(B−V) plane by Sarajedini & Layden (1997) and Ferraro et al. (1999).

Using the calibration of Carretta & Bragaglia (1998), we assumed a mean HB level $< \mathrm{V_{HB}} >$=14.15 (Harris 1996)

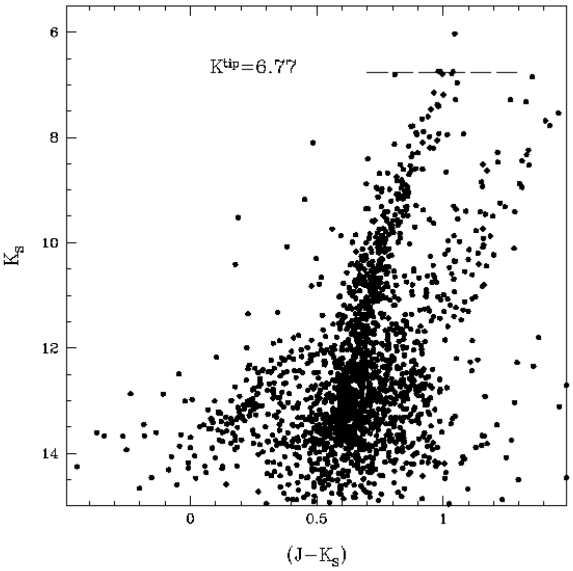

Figure 11. Infrared M22 CMD. The dashed line indicate the putative position of the RGB-Tip.

and used the V,(V−I) mean ridge line derived in Section 2.3, obtaining $[\mathrm{Fe/H}]_{\mathrm{CG}} = -1.63$ and $E(B-V) = 0.36$ (we also derived $(\mathrm{V\text{-}I})_{0,g}$=0.92 and $\Delta\mathrm{V}_{1.2}$=2.19)[9]. Using the calibration by Ferraro et al. (1999), we adopted the V_{ZAHB} just derived and used the V,(B−V) mean ridge line, obtaining $[\mathrm{Fe/H}]_{\mathrm{CG}} = -1.73$ and $E(B-V) = 0.39$ (we also derived $(\mathrm{B\text{-}V})_{0,g}$=0.73 and $\Delta\mathrm{V}_{1.2}$=2.68)

Since the two above reddening determinations are in good agreement with each other, we will adopt their average for the rest of this article:

$$E(B-V) = 0.38 \pm 0.02$$

Our determination of the reddening is identical to the one by Richter, Hilker, & Richtler (1999) which is also the most recent determination. Other estimates of the reddening range from E(B−V)=0.32 to 0.42 and can be found in Hesser (1976); Harris & Racine (1979); Harris (1996) and Crocker (1988). These values are in broad agreement with our determination within the errors, if we take into account the presence of a strong differential reddening in direction of M 22 (see previous section).

The average metallicity of M 22 can also be derived from the optical-infrared CMDs V,(V−K_S) and K_S,(J−K_S) using the RGB intrinsic colors $(\mathrm{V}-\mathrm{K}_S)_0$ and $(\mathrm{J}-\mathrm{K}_S)_0$, measured

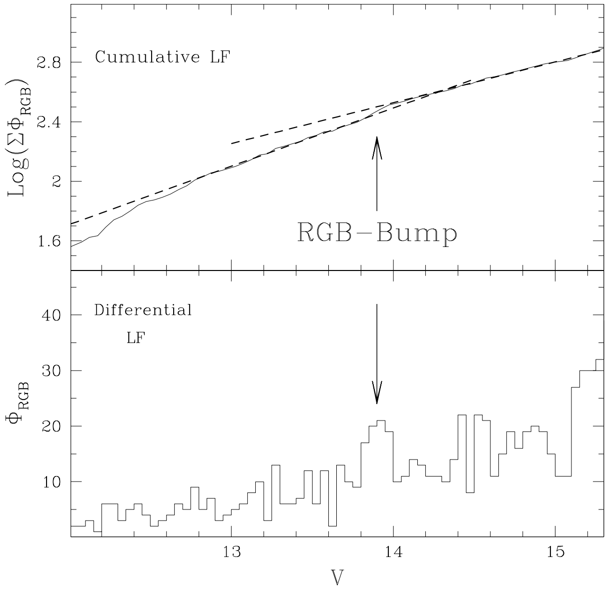

Figure 12. Differential (lower panel) and cumulative (upper panel) luminosity functions for stars selected on the RGB of M22. The arrows indicate the location of the RGB-bump at V=13.90±0.05.

at different magnitude levels (see the definition of these parameters in Ferraro et al. 2000). We used the calibrations of Valenti et al. (2004, in preparation) to yield metallicities in the Carretta & Gratton (1997) scale from the infrared photometry in the 2 MASS photometric system. We corrected our optical-infrared CMD using $E(B-V) = 0.38$ and the $(\mathrm{m}-\mathrm{M})_0$ derived below. This way we obtained different photometric metallicity estimates for M 22, which produce an average value of: $[\mathrm{Fe/H}]_{\mathrm{CG}} = -1.68$.

Averaging together all the optical and infrared metallicity determinations we obtained:

$$[\mathrm{Fe/H}]_{\mathrm{CG}} = -1.68 \pm 0.15$$

This value is in agreement, within the errors, with the most recent spectroscopic and photometric works which provide mean metallicities of -1.55, -1.48 (Lehnert, Bell, & Cohen 1991; Carretta & Gratton 1997, respectively) and -1.62 (Richter, Hilker, & Richtler 1999).

An estimate of the global metallicity can be now derived according to the prescription of Salaris, Chieffi, & Straniero (1993):

$$[\mathrm{M/H}] = [\mathrm{Fe/H}] + \log(0.638 \cdot 10^{[\alpha/\mathrm{Fe}]} + 0.362) = -1.47$$

by assuming $[\alpha/\mathrm{Fe}]$=+0.30 (Salaris & Cassisi 1996). The distance modulus is derived from the comparison of the observed value of the ZAHB obtained above ($V_{ZAHB} = 14.33 \pm 0.05$) and the absolute level computed from the Straniero, Chieffi, & Limongi (1997) models (see Eq 4 by Ferraro et al. 1999). From this relation and the global metallicity computed above ($[\mathrm{M/H}] = -1.47$) we get $M_V^{ZAHB} = 0.59$. From this figure we derived an apparent distance modulus

$$(m-M)_V = 13.74 \pm 0.2$$

---

[9] $(\mathrm{V\text{-}I})_{0,g}$ and $(\mathrm{B\text{-}V})_{0,g}$ are the dereddened RGB colors at the level of the HB, while $\Delta\mathrm{V}_{1.2}$ is the difference in V between the HB and the RGB at a dereddened color 1.2 (i.e., $(\mathrm{V\text{-}I})_0$=1.2 and $(\mathrm{B\text{-}V})_0$=1.2, see Sarajedini 1994; Ferraro et al. 1999).

and finally (using E(B−V)=0.38), an intrinsic distance modulus (m-M)$_0$=12.56 ± 0.2 which corresponds to a distance of $\sim$ 3.2 Kpc. A conservative uncertainty of 0.2 mag is assumed. Our $(m-M)_V$ is about 0.15 mag fainter than the value reported by Harris (1996). Therefore the two distance moduli are in agreement within the uncertainties, however a systematic difference between the Harris (1996) distance scale and distances derived by our semi-empirical procedure still remains and is further discussed in Ferraro et al. (1999).

As a consistency check for the parameters derived until now, we derived the putative position of the RGB-tip, in the K band. From the relations provided by Ferraro et al. (2000) and assuming the [Fe/H]$_{CG}$ just derived, we obtained as absolute magnitude of the RGB-tip:

$$M_K^{tip} = -5.93$$

Then, using the (m-M)$_0$ and E(B−V) we derived the predicted position for the RGB-Tip in apparent magnitude:

$$K^{tip} = 6.77$$

In Fig. 11 the K$_S$,(J−K$_S$) CMD of M 22 is plotted. Even if the presented CMD does not possess enough stars in the upper RGB for a safe determination of the RGB-Tip, it is nevertheless clear that the predicted RGB-tip is very similar to the magnitude at which the star counts drop to zero, K$_S$ $\simeq$6.74.

The last important feature that we were able to measure on the RGB of M 22 is the so-called RGB-bump. This feature was one of the first successful predictions of the stellar evolution theory (Thomas 1967; Iben 1968), identified observationally in 47 Tuc and subsequently in all the properly observed clusters (King et al. 1985; Fusi Pecci et al. 1990; Ferraro et al. 1999; Zoccali et al. 1999; Ferraro et al. 2000; Cho & Lee 2002), both in the optical and infrared filters. Recently, the RGB-bump was also observed in a few satellites of the Milky Way (Monaco et al. 2002; Bellazzini et al. 2002, and references therein).

As demonstrated by Fusi Pecci et al. (1990), the change in slope of the integrated luminosity function is the safest way to identify the RGB-bump location, since it makes use of stars contained in several magnitude bins. We thus identified the RGB-bump of M 22 in the V band, as shown in Fig. 12:

$$V^{bump} = 13.90 \pm 0.05$$

We also identified the RGB-bump in the K$_S$ band, finding a value in good agreement with Cho & Lee (2002).

In Figure 13 the difference of V^{bump} and V$_{ZAHB}$, ΔV_{HB}^{bump} versus [Fe/H] in the Carretta & Gratton (1997) scale, is plotted for the 42 clusters of Ferraro et al. (1999, small empty squares) and for M 22 (big filled circle). As can be seen, M 22 matches quite well the empirical calibration of Ferraro et al. (1999).

5 VARIABLE STARS AND PECULIAR OBJECTS

M 22 is known to host various type of variable stars, from the RR Lyrae stars typical of globular clusters (Wehlau & Hogg 1978) to rather peculiar or rare objects such as a type II cepheid, one sdB star (Wehlau & Hogg 1978; Kaluzny & Thompson 2001) and a Planetary Nebula (see

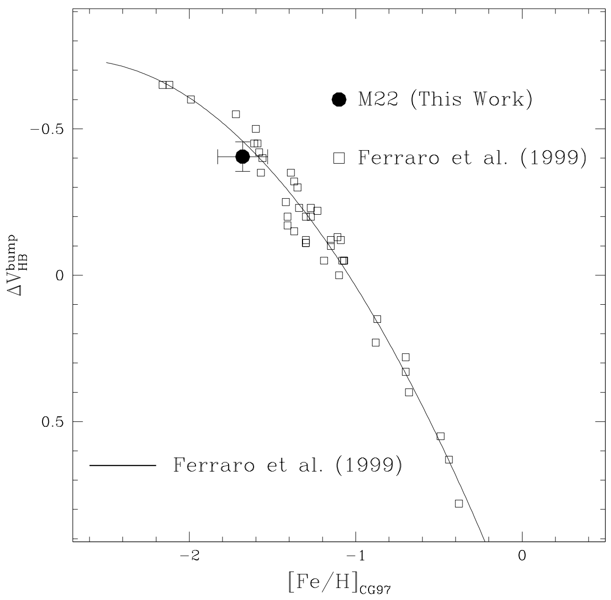

Figure 13. The magnitude of the M 22 RGB-bump (large filled circle) is compared with that of other globular clusters and with the empirical calibration of Ferraro et al. (1999) in the ΔV_{HB}^{bump} *vs* [Fe/H]$_{CG97}$ plane.

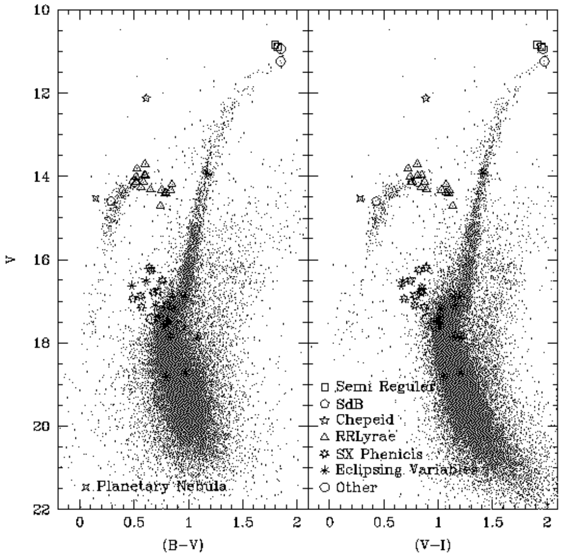

Figure 14. The position of the variable stars recovered in our catalogue is plotted in the optical CMDs. Different classes of variables have been plotted using different symbols.

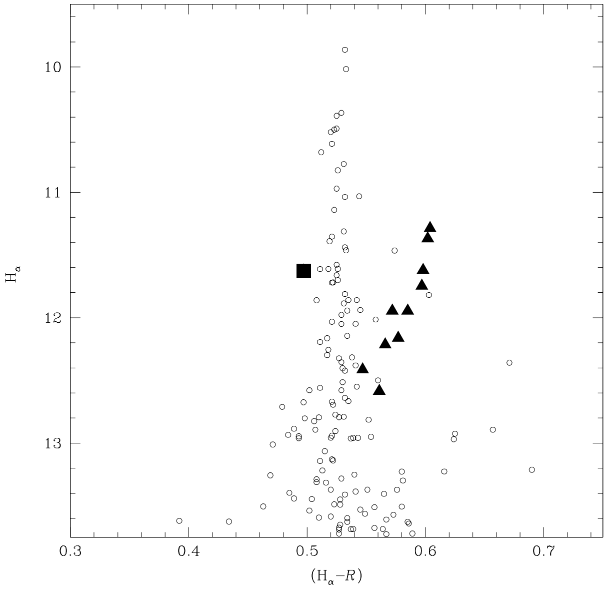

Figure 15. (H_α; $H_\alpha - \Re$) CMD for M 22 stars lying within 150 pixels from $S_\star$ (small empty circles). $S_\star$, the optical counterpart of the PN in M 22, is represented as a large filled square, while stars in the HB phase are plotted as filled triangles.

next section). A probable dwarf nova in outburst phase has also been recently identified (Anderson et al. 2003) as well as a population of X-ray sources (Webb, Gendre, & Barret 2002). In spite of the modest number of Blue Straggler stars, M 22 contains also a significant number of SX Phoenicis variables (Kaluzny & Thompson 2001).

We cross-correlated our catalogue with that of variable stars by Clement et al. (2001) which provides coordinates, classification and other useful information for all the known variable stars in M 22. In Fig. 14 we used various symbols to show the position in the CMD of the various type of variables successfully identified in our photometry. 51 variables over the 79 known in M 22 have been identified. Among them, 16 are RR Lyrae stars. Averaging the V magnitudes of the RR Lyrae observed at random phase in our photometry we obtain V_{HB}=14.17±0.25. This value for the HB magnitude is about 0.15 magnitude brighter than our estimate of V_{ZAHB} in qualitative agreement to what expected from equation #2 by Ferraro et al. (1999).

5.1 The Planetary Nebula in M22

Together with Pal 6, NGC 6441 and M 15 (Jacoby et al. 1997; Adams et al. 1984), M22 is one of the few galactic globular clusters which are known to host a planetary nebula (PN). It was first discovered with the IRAS satellite by Gillett et al. (1986) as a pointlike source (IRAS 18333-2357) and then identified as a Planetary Nebula (Gillett et al. 1989). The central star of the PN has also been identified (Gillett et al. 1989), as a blue star (the *"southern component"*, hereafter $S_\star$) belonging to a pair which lies only $\sim 2''$ away from the infrared source.

Some of the physical properties of the PN and its central star were derived by Cohen & Gillett (1989). Considering the expansion velocity (11 km/s) of the nebula and assuming that its size corresponds to the distance to $S_\star$, Cohen & Gillett (1989) concluded that the age of the PN appears to be only $\simeq$ 6000 yr. This short time scale implies that the central star should still be quite bright, with a luminosity comparable to that of the RGB-tip. This poses an apparent problem, since $S_\star$ has a magnitude (and even colors) comparable to that of a slightly evolved HB star, as can be seen in Fig. 14.

To further investigate the photometric properties of $S_\star$, we constructed the instrumental (non-calibrated) H_α,($H_\alpha - \Re$) CMD for stars contained in a circle with a radius of 150 pixels, centered on $S_\star$ (Fig. 15). In this diagram, RGB stars occupy a vertical sequence while genuine HB stars (filled triangles), which have a more pronounced H_α absorption, tend to have redder ($H_\alpha - \Re$) colors. In the same diagram, $S_\star$ (large filled square) shows a moderate H_α excess, with ($H_\alpha - \Re$) slightly bluer than the normal RGB stars and very different from the HB stars. This is in agreement with the substantial amount of hydrogen emission displayed by the spectrum of $S_\star$ (Harrington & Paltoglou 1993), consistent with what expected if $S_\star$ is the central star of a newborn PN.

We thus need to explain the unusual position of $S_\star$ in the V,(B−V) diagram. An enlargement of the CMD around $S_\star$ is shown in Fig. 16 (upper panel), where the theoretical isochrone of a post-AGB star with t$\simeq$12.5 Gyr and Z=0.0004 has been also overplotted (Bertelli et al. 1994). Clearly, the position of $S_\star$ (large filled square) is not compatible with the isochrone. However, $S_\star$ should be surrounded by nebular dust, which causes an excess of reddening of about ΔE(B-V)$\simeq$0.14 (Cudworth 1990; Harrington & Paltoglou 1993). After applying the corresponding correction, the position of $S_\star$ is reconciled with the isochrone (large filled circle in Fig. 16, upper panel).

The theoretical ($\log T_{eff}$,$\log L/L_\odot$) plane can also provide useful insight into the evolutionary state of $S_\star$ and its compatibility with a post AGB-star of about 6000yr. Spectroscopic studies derive for $S_\star$ a temperature of 50,000$\leqslant T_{eff} \leqslant$75,000 K (Cohen & Gillett 1989; Harrington & Paltoglou 1993). In this range of temperatures, the bolometric correction in the V band, BC_V, varies between -4.08 and -5.30, using a blackbody model (Origlia & Leitherer 2000). If we assume T_{eff}=60,000 K (hence BC_V=-4.62), ΔE(B-V)$\simeq$0.14 and $(m-M)_V$=13.75, then $S_\star$ occupies the position marked by a large filled circle in the lower panel of Fig. 16. We also overplotted the theoretical post-AGB evolutionary track for a 1 $M_\odot$ and Z=0.001 star (Vassiliadis & Wood 1994). Tiny empty dots mark the positions occupied by stars of 5500, 6900 and 8300 yr. As can be seen, $S_\star$ closely matches the track at a luminosity comparable to that of the RGB-tip and a temperature which is fully compatible with the central star of a PN of ~6000 yr.

We thus have been able to add supporting evidence to the identification of $S_\star$ as the central star of the planetary nebula IRAS 18333-2357 in M 22.

6 SUMMARY AND CONCLUSIONS

We presented a wide field (33′×34′), multi-band photometry (B, V, I, H_α and the adjacent continuum, $\Re$) of the globular

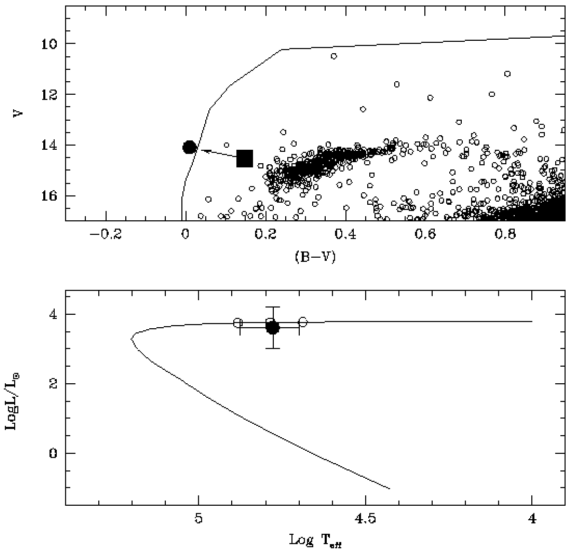

Figure 16. Upper panel: zoomed CMD in the HB region. The position of $S_\star$ is marked as a filled square. The filled circle represents the putative position of $S_\star$ if a reddening excess of ΔE(B-V)$\simeq$0.14 is assumed. The continuous curve is a post-AGB theoretical isochrone with t$\simeq$12.5 Gyr and Z=0.0004. Lower panel: The position of $S_\star$ in the absolute plane, once applied the bolometric correction, is plotted (filled circle). The continuous curve is a theoretical post-AGB evolutionary track for a 1 M$_\odot$ and Z=0.001 star. Empy circles mark evolutionary steps between 5000 and 8300 years.

cluster M 22. For the H$_\alpha$ and $\Re$ filters we presented only instrumental magnitudes in a tiny area around the PN in M 22. We provided the astrometrically calibrated catalog containing B, V and I calibrated magnitudes for ∼140,000 stars covering an area of $\sim24'\times33'$. About 2000 stars in our catalog have been also measured in the near infrared by the 2 MASS survey, providing calibrated J, H and K$_S$ magnitudes in addition to our five optical bands.

We use this catalog to characterize the evolved stellar sequences in M 22, especially the RGB, by deriving mean ridge lines in the optical and infrared colors, and by measuring the V magnitude of the RGB-bump, which appears in good agreement with the most recent calibration versus metallicity (Ferraro et al. 1999). We also derived the mean metallicity, reddening and distance moduli, in a self-consistent way. The derived values agree well with previous determinations.

Profiting from our multi-band catalogue, we re-examined the problem of the metallicity spread in M 22. We demonstrated the presence of differential reddening, confirming earlier findings (Richter, Hilker, & Richtler 1999, and references therein). We also conclude that, according to our photometric measurements, most of the intrinsic width of the RGB must be due to differential reddening, while the maximum metallicity spread allowed by our data is Δ[Fe/H]$\simeq$ 0.1 $\div$ 0.2 dex, i.e., compatible with the photometric errors.

We finally identified most of the variable stars and peculiar objects known in the observed field of M 22. In particular, we provided additional evidence supporting the optical identification of the central star in the planetary nebula IRAS 18333-2357, one of the few identified in a GGC up to now.

ACKNOWLEDGMENTS

We are grateful to L. Origlia and E. Valenti for useful suggestions and discussions. We also thank an anonymous referee for useful comments that have substantially improved our paper. This research is partially supported by MIUR (Ministero della Istruzione, dell'Università e della Ricerca) and ASI (Agenzia Spaziale Italiana). Part of the data analysis has been performed using software packages developed by P. Montegriffo at the Osservatorio Astronomico di Bologna.

REFERENCES

Adams, S., Seaton, M. J., Howarth, I. D., Auriere, M., & Walsh, J. R. 1984, MNRAS, 207, 471

Albrow, M. D., De Marchi, G., & Sahu, K. C. 2002, ApJ, 579, 660

Anderson, J., Cool, A. M., & King, I. R. 2003, ApJ, 597, L140

Anthony-Twarog, B. J., Twarog, B. A., & Craig, J. 1995, PASP, 107, 32

Arp, H. C. & Melbourne, W. G. 1959, AJ, 64, 28

Bellazzini, M., Ferraro, F. R., Origlia, L., Pancino, E., Monaco, L., & Oliva, E. 2002, AJ, 124, 3222

Bertelli, G., Bressan, A., Chiosi, C., Fagotto, F., & Nasi, E. 1994, A&AS, 106, 275

Brown, J. A. & Wallerstein, G. 1992, AJ, 104, 1818

Cannon, R. D. 1980, A&A, 81, 379

Carpenter, J. M. 2001, AJ, 121, 2851

Carretta, E. & Bragaglia, A. 1998, A&A, 329, 937

Carretta, E. & Gratton, R. G. 1997, A&AS, 121, 95

Cho, D. & Lee, S. 2002, AJ, 124, 977

Clement, C. M. et al. 2001, AJ, 122, 2587

Cohen, J. G. 1981, ApJ, 247, 869

Cohen, J. G. & Gillett, F. C. 1989, ApJ, 346, 803

Crocker, D. A. 1988, AJ, 96, 1649

Cudworth, K. M. 1990, AJ, 99, 1863

Da Costa, G. S. & Armandroff, T. E. 1990, AJ, 100, 162

Davidge, T. J. & Harris, W. E. 1996, ApJ, 462, 255

Davidge, T. J. & Harris, W. E. 1995, ApJ, 445, 211

Dean, J.F., Warren, P.R., & Cousins, A.W., 1978, MNRAS, 183, 569

Dickens, R. J. & Woolley, R. v. d. R. 1967, Royal Greenwich Observatory Bulletin, 128, 255

Elias, J. H., Frogel, J. A., Matthews, K., & Neugebauer, G. 1982, AJ, 87, 1029

Ferraro, F. R., Fusi Pecci, F., & Buonanno, R. 1992, MNRAS, 256, 376

Ferraro, F. R., Carretta, E., Corsi, C. E., Fusi Pecci, F., Cacciari, C., Buonanno, R., Paltrinieri, B., & Hamilton, D. 1997, A&A, 320, 757

Ferraro, F. R., Messineo, M., Fusi Pecci, F., de Palo, M. A., Straniero, O., Chieffi, A., Limongi, M.

Ferraro, F.R., Montegriffo, P., Origlia, L., & Fusi Pecci, F., 2000, AJ, 119, 1282

Ferraro, F. R., D'Amico, N., Possenti, A., Mignani, R. P., & Paltrinieri, B. 2001, ApJ, 561, 337

Fusi Pecci, F., Ferraro, F. R., Crocker, D. A., Rood, R. T., Buonanno, R. 1990, A&A, 238, 95

Gillett, F. C., Backman, D. E., Beichman, C., & Neugebauer, G. 1986, ApJ, 310, 842

Gillett, F. C., Jacoby, G. H., Joyce, R. R., Cohen, J. G., Neugebauer, G., Soifer, B. T., Nakajima, T., & Matthews, K. 1989, ApJ, 338, 862

Gratton, R. G. 1982, A&A, 115, 171

Gratton, R. G. & Ortolani, S. 1989, A&A, 211, 41

Harrington, J. P. & Paltoglou, G. 1993, ApJ, 411, L103

Harris, W. E. 1996, VizieR Online Data Catalog, 7195

Harris, W. E. & Racine, R. 1979, ARA&A, 17, 241

Hesser, J. E., Hartwick, F. D. A., & McClure, R. D. 1977, ApJS, 33, 471

Hesser, J. E. 1976, PASP, 88, 849

Iben, I. Jr. 1968, Nature, 220, 143

Jacoby, G. H., Morse, J. A., Fullton, L. K., Kwitter, K. B., & Henry, R. B. C. 1997, AJ, 114, 2611

Kaluzny, J. & Thompson, I. B. 2001, A&A, 373, 899

King, C. R., Da Costa, G. S., & Demarque, P. 1985, ApJ, 299, 674

Laird, J. B., Wilhelm, R. J., & Peterson, R. C. 1991, ASP Conf. Ser. 13: The Formation and Evolution of Star Clusters, 578

Landolt, A. U. 1992, AJ, 104, 340

Lee, J. & Carney, B. W. 1999, AJ, 117, 2868

Lehnert, M. D., Bell, R. A., & Cohen, J. G. 1991, ApJ, 367, 514

Manduca, A. & Bell, R. A. 1978, ApJ, 225, 908

Monaco, L., Ferraro, F. R., Bellazzini, M., & Pancino, E. 2002, ApJ, 578, L47

Norris, J. & Freeman, K. C. 1983, ApJ, 266, 130

Origlia, L. & Leitherer, C. 2000, AJ, 119, 2018

Peterson, R. C. 1980, IAU Symp. 85: Star Formation, 85, 461

Pilachowski, C., Leep, E. M., Wallerstein, G., & Peterson, R. C. 1982, ApJ, 263, 187

Piotto, G. & Zoccali, M. 1999, A&A, 345, 485

Richter, P., Hilker, M., & Richtler, T. 1999, A&A, 350, 476

Rosenberg, A., Piotto, G., Saviane, I., & Aparicio, A. 2000, A&AS, 144, 5

Sahu, K. C., Casertano, S., Livio, M., Gilliland, R. L., Panagia, N., Albrow, M. D., & Potter, M. 2001, Nature, 411, 1022

Salaris, M. & Cassisi, S. 1996, A&A, 305, 858

Salaris, M., Chieffi, A., & Straniero, O. 1993, ApJ, 414, 580

Sarajedini, A. 1994, AJ, 107, 618

Sarajedini, A. & Layden, A. 1997, AJ, 113, 264

Savage, B. D. & Mathis, J. S. 1979, ARA&A, 17, 73

Shapley, H. 1930, Harvard College Observatory Bulletin, 874, 4

Stetson, P. B. 1987, PASP, 99, 191 1999, AJ, 118, 1738

Straniero, O., Chieffi, A., & Limongi, M. 1997, ApJ, 490, 425

Thomas, H.-C. 1967, Z. Astrophys, 67, 420

Valenti, E., Ferraro, F. R. and Origlia, L. 2004, in preparation

Vassiliadis, E. & Wood, P. R. 1994, VizieR Online Data Catalog, 209, 20125

Webb, N. A., Gendre, B., & Barret, D. 2002, A&A, 381, 481

Wehlau, A. & Hogg, H. S. 1978, AJ, 83, 946

Woolley, R. R. 1966, Royal Observatory Annals, 2, 1

Zinn, R. & West, M. J. 1984, ApJS, 55, 45

Zoccali, M., Cassisi, S., Piotto, G., Bono, G., & Salaris, M. 1999, ApJ, 518, L49